

Growth-induced delamination of an elastic film adhered to a cylinder

Mathematics and Mechanics of Solids
1–16

© The Author(s) 2024

Article reuse guidelines:

sagepub.com/journals-permissions

DOI: 10.1177/10812865231209412

journals.sagepub.com/home/mms

**Giuseppe Bevilacqua**

DSFTA, Università di Siena, Siena, Italy

Gaetano Napoli 

Dipartimento di Matematica e Applicazioni “R. Caccioppoli”, Università degli Studi di Napoli Federico II, Naples, Italy

Stefano Turzi

Dipartimento di Matematica, Politecnico di Milano, Milano, Italy

Received 23 July 2023; accepted 6 October 2023

Abstract

We study the delamination induced by the growth of a thin adhesive sheet from a cylindrical, rigid substrate. Neglecting the deformations along the axis of the cylinder, we treat the sheet as a one-dimensional flexible and compressible ring, which adheres to the substrate by capillary adhesion. Using the calculus of variations, we obtain the equilibrium equations and in particular arrive at a *transversality condition* involving in a non-trivial way the curvature of the substrate, the extensibility of the ring and capillary adhesion. By numerically solving the equilibrium equations, we show that delamination by growth occurs through a discontinuous transition from the fully adherent solution to the partially delaminated one. The shape of the delaminated part can take the form either of a *ruck*, with a small slope, or a *fold*, with a large slope. Furthermore, in the weak adhesion regime, complete delamination may occur. We construct the phase diagram between the different solutions in the parameter space. In the quasi-incompressible limit, numerical results are also supported by asymptotic calculations both in the strong and weak adhesion regimes.

Keywords

Delamination, snap-through buckling, capillary adhesion, transversality condition

1. Introduction

In everyday experience, the peeling of adhesive films from both hard and soft, curved substrates is a fairly recurring event. Although, for example, the formation of a wrinkle on a bottle label has trivial consequences, the delamination of thin films becomes a more significant issue for coating technologies such as stretchable electronics [1–3]. Thus, understanding the mechanics of adhesive sheets becomes crucial for applications, but

Corresponding authors:

Gaetano Napoli, Dipartimento di Matematica e Applicazioni “R. Caccioppoli”, Università degli Studi di Napoli “Federico II”, Complesso Monte S. Angelo, Napoli, 80126, Italy.

Email: gaetano.napoli@unina.it

also provides an interesting mathematical paradigm in which mechanics of slender bodies, adhesion properties and substrate geometry meet [4].

Delaminated blisters originate in compressed films [5, 6]. This compression may be due to external compressive forces applied to the edge of the sheet, or to the growth of the sheet when it is confined, or to thermal dilation.

Delamination blister formation is a classic problem, in pioneering works the analysis was limited to blisters with a small slope in the realm of small deformations theory. However, in many new applications, this limitation is inappropriate and many subsequent studies modeled thin films as nonlinear Euler's Elasticae [7–9], allowing large deflections to be handled. Moreover, the occurrence of delamination blister has been studied extensively over the last two decades in a variety of situations with both inextensible and extensible rods adhered to flat adhesive substrates [10–15], considered either rigid or soft.

Delamination also occurs when flexible rings are confined within a small container, whether rigid or flexible, both in the presence or absence of adhesion [10, 16–19]. In these cases, the curvature of the confining wall affects the equilibrium shape by promoting the regions of adhesion, acting as an effective adhesion.

In an inextensible sheet, the transition to a delaminated shape from a flat or concave substrate requires an infinite compressive force [20]. In contrast, if a small compression of the sheet is allowed, the compressive force remains finite and delamination occurs via a discontinuous transition to a blister of finite amplitude [12, 13, 17].

In this work, we study the delamination of a compressible thin film that adheres to the outer surface of a cylinder by capillary action. The aim of the paper is to extend results obtained for a compressible adhesive sheet on a flat substrate to a circular substrate [13, 18], in the same time it generalizes the problem of a compressible film in contact with a curved surface [17] in presence of capillary adhesion. Extensibility and adhesion play a role in defining the two key characteristic lengths of the model, namely, ℓ_b that relates bendability to extensibility, and the elastocapillary length ℓ_{ec} that relates bendability to adhesion. We show how the physical features of the transition depend on the values of ℓ_b , ℓ_{ec} and the radius of the cylinder r and derive the phase diagrams for different values of the ratios ℓ_b/r and ℓ_{ec}/r .

By comparing the stored energies of the adhered state, the small-slope ruck (Figure 1(c)), and the fold configuration (Figure 1(d)), we determine the possible behaviors of growing thin sheet. In the nearly-incompressible case, when the adhesion is sufficiently strong, i.e., $\ell_b \ll \ell_{ec} \ll r$, we find that the film delaminates into a small-slope ruck, which then grows and finally turns into a large-slope fold, when $\ell_b = 10^{-5/2}r$, while the film delaminates directly into a large slope fold, when $\ell_b = 10^{-3/2}r$. Finally, when the adhesion is weak ($\ell_{ec} \gg r$), we only observe a transition to a ruck which then develops to a completely delaminated solution (Figure 1(b)) as the film grows.

The article is organized as follows. In section 2, we posit the energy functional of the model from which we derive the equilibrium equations and the boundary conditions in section 3. The variational approach provides a novel transversality condition at the detachment point, which combines the intrinsic lengths in a non-trivial way. In section 4, we discuss the main results of our theory, and compare the numerical results with the asymptotic approximations, as derived in Appendix 1. Finally, in section 5, we draw the conclusions.

2. Energy functional

We consider an infinite cylinder of radius r , covered with a tape of natural length L , naturally straight. We assume the tape to be compressible, i.e., its length may change when the tape is deformed. Furthermore, the length of the rod can change as the rod grows, which corresponds to varying L .

The geometry of the curve is described by the position vector $\mathbf{r}(S) = [x(S), y(S)]$, where S is the referential arc-length. The unit tangent and unit normal to the curve are given by $\boldsymbol{\tau}(S) = [\cos \theta(S), \sin \theta(S)]$ and $\mathbf{v}(S) = [-\sin \theta(S), \cos \theta(S)]$, where $\theta(S)$ is the counter-clockwise angle between the x -axis and the tangent. Since we consider extensible rods, it is convenient to introduce also the local stretch $\lambda(S) := \|\mathbf{r}'(S)\|$. Furthermore, we denote with \mathbf{e}_α the unit tangent to the circular substrate forming an angle α with the x -axis (see Figure 2).

We derive the equilibrium equations, and the boundary conditions for the partial delaminated solution, by imposing stationarity of the energy functional which comprises two parts: the energy of the detached region W_f and the energy of the adhered region W_a , where

$$W_f = \int_0^{\bar{S}} w_f dS, \quad W_a = \int_{\bar{S}}^{\frac{L}{2}} w_a dS \quad (1)$$

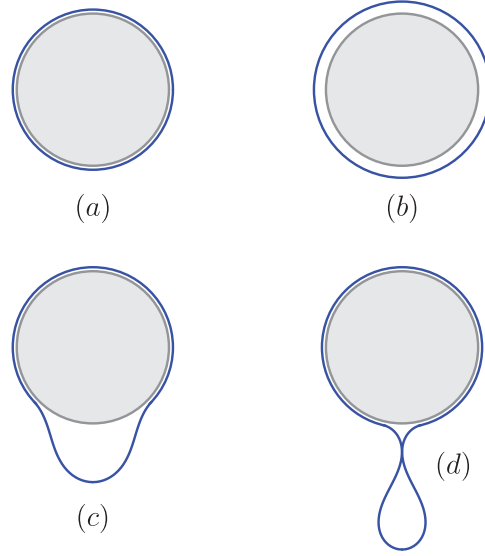


Figure 1. Schematic representation of the film profiles: (a) fully adhered configuration, (b) fully delaminated, (c) ruck, and (d) fold.

with

$$w_f = k (\theta')^2 + b(\lambda - 1)^2 + 2\mathbf{n} \cdot (\mathbf{r}' - \lambda \boldsymbol{\tau}), \quad (2a)$$

$$w_a = k \frac{\lambda^2}{r^2} + b(\lambda - 1)^2 + 2\mathbf{n} \cdot (\mathbf{r}' - \lambda \mathbf{e}_\alpha) - 2\lambda \Delta\gamma. \quad (2b)$$

Both w_f and w_a account for a bending term, proportional to the bending rigidity k , and a strain energy, proportional to the compression modulus b . The quantity

$$\ell_b := \sqrt{\frac{k}{b}}$$

defines a characteristic length. Since $b = EA$ and $k = EI$, being E is the elastic modulus of the material, A is the area of the film cross-section, and I is the second moment of area of the sheet cross-section, the intrinsic length ℓ_b turns out to be of the order of the thickness of the strip.

The last term in equation (2a) enforces the constraints

$$x' = \lambda \cos \theta, \quad y' = \lambda \sin \theta, \quad (3)$$

which translate the assumption that the rod is extensible but unsharable. The vector \mathbf{n} is a Lagrange multiplier representing the rod's internal force [21].

The last term in the energy density (2b) is an adhesion-promoting term, proportional to the adhesion area through the constant $\Delta\gamma$, the sheet-substrate adhesion energy density. Thus, a further intrinsic characteristic length can be defined

$$\ell_{ec} := \sqrt{\frac{k}{\Delta\gamma}}, \quad (4)$$

which is called the elastocapillary length.

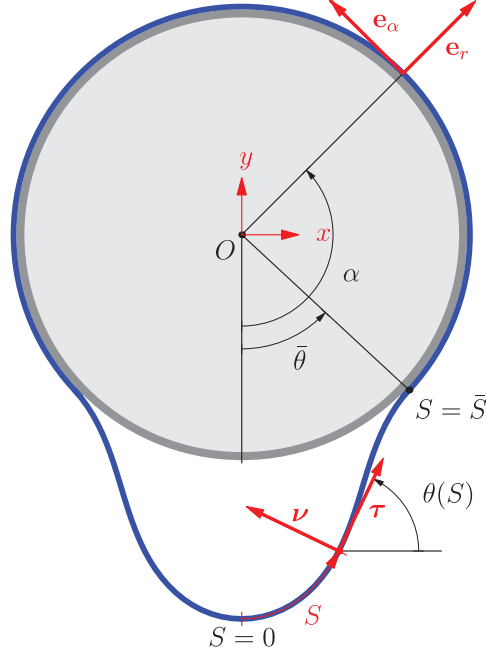


Figure 2. Schematic representation of the elastic film in contact with the outer surface of a cylinder of radius r . We assume mirror symmetry with respect to the y -axis. The free part of the curve is parameterised by values of the referential arc length $S \in [0, \bar{S}]$, where \bar{S} corresponds to the detachment point.

3. Equilibrium equations

Let us consider h , η , and \mathbf{u} be the variations of θ , λ , and \mathbf{r} , respectively. Within the free region, the variation h , η , and \mathbf{u} are arbitrary, so that we obtain

$$\begin{aligned} \delta W_f = \int_0^{\bar{S}} \left[\left(\frac{\partial w_f}{\partial \theta} - \left(\frac{\partial w_f}{\partial \theta'} \right)' \right) h + \frac{\partial w_f}{\partial \lambda} \eta \right. \\ \left. - \left(\frac{\partial w_f}{\partial \mathbf{r}'} \right)' \cdot \mathbf{u} \right] dS + \left(\frac{\partial w_f}{\partial \theta'} \right)_{\bar{S}^-} \bar{h}^- + \left(\frac{\partial w_f}{\partial \mathbf{r}'} \right)_{\bar{S}^-} \cdot \bar{\mathbf{u}}^- + \bar{w}_f^- \delta \bar{S}, \end{aligned} \quad (5)$$

where bar above the variables denotes that these variables are calculated in $S = \bar{S}$. A superscript “minus” (respectively, “plus”) means that the corresponding function is evaluated as S approaches \bar{S} from the left (respectively, right).

It is worth noticing that $S = \bar{S}$ is not fixed and, hence, any variations at the detachment point should include a further contribute due to change of the curve length, so that

$$\delta \bar{\mathbf{r}}^- = \bar{\mathbf{u}}^- + \bar{\lambda}^- \boldsymbol{\tau}^- \delta \bar{S}, \quad (6a)$$

$$\delta \bar{\theta}^- = \bar{h}^- + (\bar{\theta}')^- \delta \bar{S}. \quad (6b)$$

The virtual displacement in the adhered region is purely tangential to the ring, i.e., $\mathbf{u} = u_\alpha \mathbf{e}_\alpha$, where \mathbf{e}_α is the unit tangent to the substrate, so that

$$\delta W_a = \int_{\bar{S}}^{\frac{L}{2}} \left[\frac{\partial w_a}{\partial \lambda} \eta - \left(\frac{\partial w_a}{\partial \mathbf{r}'} \right)' \cdot \mathbf{e}_\alpha u_\alpha \right] dS - \left(\frac{\partial w_a}{\partial \mathbf{r}'} \cdot \mathbf{e}_\alpha \right)_{\bar{S}^+} \bar{u}_\alpha^+ - \bar{w}_a^+ \delta \bar{S}. \quad (7)$$

Since the detachment point lies on a given curve (in our case a circumference), its virtual displacement can be due to either a longitudinal deformation of the rod (which occurs when the rod is stretched but material points

in contact with the substrate do not change and \bar{S} remains fixed) or to a change in the contact point (which can occur even if the rod is unstretched). Summing these two contributions, we get

$$\delta\bar{\mathbf{r}}^+ = (\bar{\mathbf{u}}^+ \cdot \mathbf{e}_\alpha + \bar{\lambda}^+ \delta\bar{S})\mathbf{e}_\alpha. \quad (8)$$

Note that, since the angle $\pi - \bar{\theta}$ subtends half of the adhered arc, the length of the adhered curve can be expressed as

$$r(\pi - \bar{\theta}) = \int_{\bar{S}}^{\frac{L}{2}} \lambda dS, \quad (9)$$

whence

$$r\delta\bar{\theta}^+ = - \int_{\bar{S}}^{\frac{L}{2}} \delta\lambda dS + \bar{\lambda}^+ \delta\bar{S}. \quad (10)$$

Using equations (6b) and (10), with the requirement that $\delta\bar{\theta}^- = \delta\bar{\theta}^+$, we get

$$\bar{h}^- = \left(\frac{\bar{\lambda}^+}{r} - (\bar{\theta}')^- \right) \delta\bar{S} - \int_{\bar{S}}^{\frac{L}{2}} \delta\lambda dS. \quad (11)$$

The requirement that the first term of δW_f vanishes for any arbitrary choice of $h(S)$, $\eta(S)$, and $\mathbf{u}(S)$, leads to equilibrium equations of the delaminated curve:

$$k\theta'' + \lambda n_y \cos \theta - \lambda n_x \sin \theta = 0, \quad (12a)$$

$$n_x \cos \theta + n_y \sin \theta - b(\lambda - 1) = 0, \quad (12b)$$

$$\mathbf{n}' = \mathbf{0}, \quad (12c)$$

which have to be supplemented with the shape equation (3). We are considering the following Dirichlet conditions in $S = 0$,

$$x(0) = 0, \quad \theta(0) = 0, \quad (13)$$

so that also the corresponding variation fields, u_x and h , vanish in $S = 0$. By contrast, we do not assume vanishing variation for the vertical component u_y , so that we obtain the free boundary condition

$$n_y(0) = 0. \quad (14)$$

This, together with equation (12c), yields $n_y(S) \equiv 0$, and we can omit n_y from equation (12).

A similar argument for the adhered region yields

$$n_\alpha - b(\lambda - 1) + \Delta\gamma + \frac{k}{r} \left(\frac{\lambda}{r} - (\bar{\theta}')^- \right) = 0, \quad (15a)$$

$$\mathbf{n}' \cdot \mathbf{e}_\alpha = 0. \quad (15b)$$

Assuming a constant λ in the adhered region, we deduce from equation (15a) that also n_α is constant. Hence, equation (15b) implies that the normal (or radial) component of \mathbf{n} vanishes.

In order to study the remaining boundary terms, we assume the continuity conditions $\delta\bar{\theta}^+ = \delta\bar{\theta}^-$ and $\delta\bar{\mathbf{r}}_\alpha^- = \delta\bar{\mathbf{r}}_\alpha^+$, where $\delta\bar{\mathbf{r}}_\alpha^\pm := \delta\bar{\mathbf{r}}^\pm \cdot \bar{\mathbf{e}}_\alpha$. Thus, the request that the coefficient of $\delta\bar{\mathbf{r}}_\alpha$ vanishes yields the continuity condition of the internal force tangential component

$$\bar{\mathbf{n}}^- \cdot \bar{\mathbf{e}}_\alpha = \bar{\mathbf{n}}^+ \cdot \bar{\mathbf{e}}_\alpha, \quad (16)$$

while the request that the $\delta\bar{S}$ coefficient vanishes leads to

$$w_f(S^-) - w_a(S^+) + \frac{\partial w_f}{\partial \theta'} \Big|_{\bar{S}} \left(\frac{\bar{\lambda}^+}{r} - (\bar{\theta}')^- \right) + \bar{n}_\alpha^+ \bar{\lambda}^+ - \bar{n}_\alpha^- \bar{\lambda}^- = 0. \quad (17)$$

Combining equations (12b), (15a), and (16), we derive $\bar{\lambda}^-$ and we replace the result into equation (17) so getting the transversality condition at the detachment point

$$(\bar{\lambda}^+ - r(\bar{\theta}')^-)^2 - \frac{2r^2\bar{\lambda}^+}{\ell_{ec}^2} + \frac{\ell_b^2}{\ell_{ec}^4 r^2} [\ell_{ec}^2 (\bar{\lambda}^+ - r(\bar{\theta}')^-) - r^2]^2 = 0. \quad (18)$$

We note that in the context of the mechanics of elastic rods, this condition has been a subject of interest for many years. A comprehensive treatment of this transversality condition for elastic rods can be found in the works of O'Reilly [22, 23], where it is derived as a balance of “material momentum” and it is considered as an independent balance law in addition to the balance of forces and moments. As such, our equation (18) can be viewed as an implicit manifestation of a balance of “material momentum”. However, we prefer here a more direct approach and derive it from a classical variational principle. Unlike the cases classically studied, our condition (18) takes into account adhesion, extensibility, and curvature of the container, the combined effect of which, to the best of our knowledge, has never been explicitly considered before.

Furthermore, at $S = \bar{S}$, the following boundary conditions hold

$$x(\bar{S}) = r \sin \bar{\theta}, \quad y(\bar{S}) = r(1 - \cos \bar{\theta}). \quad (19)$$

Note that, since in the adhered region $\lambda(S) = \bar{\lambda}^+$, equation (9) yields

$$\bar{\theta} = \pi - \frac{\bar{\lambda}^+}{r} \left(\frac{L}{2} - \bar{S} \right). \quad (20)$$

3.1. Known limiting cases

In the limit of vanishing capillary adhesion ($\ell_{ec}/r \rightarrow \infty$), the transversality condition (18) yields (see the literature [17])

$$\bar{\lambda}^+ - r(\bar{\theta}')^- = 0 \quad (21)$$

By contrast, in the inextensible case ($\ell_b = 0$, $\bar{\lambda}^+ = 1$), equation (18) reads (see also the literature [10, 16, 24])

$$(1 - r(\bar{\theta}')^-)^2 - \frac{2r^2}{\ell_{ec}^2} = 0. \quad (22)$$

Finally, the flat limit ($\bar{S}/r \rightarrow 0$ and $\ell_{ec}/r \rightarrow 0$) provides (see the literature [11, 12])

$$[(\bar{\theta}')^-]^2 - 2\frac{\bar{\lambda}^+}{\ell_{ec}^2} + \frac{\ell_b^2}{\ell_{ec}^4} = 0. \quad (23)$$

3.2. Summary of the equations

For the reader's convenience, we report here the main equations, the unknown fields, and the boundary conditions of our problem.

For the free part $S \in [0, \bar{S})$, in the absence of vertical loads on the free curve, $n_y(S) = 0$, so that the balance equations read

$$k\theta'' - \lambda n_x \sin \theta = 0, \quad (24a)$$

$$n'_x = 0, \quad (24b)$$

$$x' = \lambda \cos \theta, \quad (24c)$$

$$y' = \lambda \sin \theta, \quad (24d)$$

where the stretch $\lambda(S)$ is calculated as

$$\lambda = 1 + \frac{n_x}{b} \cos \theta. \quad (25)$$

The only unknown in the adhered region is the constant stretch ratio $\bar{\lambda}^+$, which can be calculated from the continuity of the tangential component n_α . Combining equations (15a), (16), and (25), we obtain

$$\bar{\lambda}^+ = \frac{br^2}{k + br^2} \left(\lambda(\bar{S}^-) + \frac{\Delta\gamma}{b} + \frac{k}{r} \theta'(\bar{S}^-) \right). \quad (26)$$

Finally, we also have the identity (9)

$$\bar{\theta} = \pi - \frac{\bar{\lambda}^+}{r} \left(\frac{L}{2} - \bar{S} \right). \quad (27)$$

Overall, we have four S -dependent unknowns $x(S)$, $y(S)$, $\theta(S)$, and $\theta'(S)$, and two constant unknowns \bar{S} , n_x . From these, we can reconstruct the stretch ratio $\lambda(S)$ in the free part (from equation (25)), the stretch ratio $\bar{\lambda}^+$ in the adhered region (from equation (26)), and the detachment angle $\bar{\theta}$ (from equation (27)).

The boundary conditions are

$$x(0) = 0, \quad \theta(0) = 0, \quad \theta(\bar{S}) = \bar{\theta} \quad (28a)$$

$$x(\bar{S}) = r \sin \bar{\theta}, \quad y(\bar{S}) = r(1 - \cos \bar{\theta}). \quad (28b)$$

Finally, the transversality condition (18) yields the additional equation at the boundary, necessary to close the problem.

4. Results

We study the problem for different values of the parameter L , which mimics a growth process, and for various values of the characteristic lengths r , ℓ_b , and ℓ_{ec} , which depend on the geometric and constitutive features of the system.

We will consider three different sets of possible solutions, namely (see Figure 1):

- (a) The *completely adhered* solution. This equilibrium configuration is a circumference of radius r , fully in contact with the substrate. The tape is uniformly strained/compressed, with

$$\lambda_{\text{adh}} = 2\pi \frac{r}{L}. \quad (29)$$

- (b) The *fully delaminated* solution is represented by a circumference, with no contact point with the substrate. This solution is admitted only if $R \geq r$, where $R = L/(2\pi)$.
- (c), (d) *Partially delaminated* configurations, where the detached region is a symmetric blister of referential length $2\bar{S}$. The shape of this blister depends on R/r , on the constitutive parameters of the tape and on the capillary adhesion $\Delta\gamma$. We distinguish between two partially delaminated solutions: a *ruck* (see Figure 1(c)), i.e., a small-slope delamination where opposite sides of the rod do not touch each other, and a *fold* (see Figure 1(d)), in which the rod undergoes large-slope deformation with self-contact.

We have studied the problem by numerically solving equations (24) with the corresponding boundary conditions (28a) and (18), using the MATLAB function `bvp4c`, for several values of the parameters. A first feature of the solutions is that, given ℓ_b , the detachment angle $\bar{\theta}$ as a function of the excess-length ϵ ,

$$\epsilon := \frac{L - 2\pi r}{2\pi r}, \quad (30)$$

has two characteristic trends that depend on the value of ℓ_{ec} . For *weak* capillary-strength, i.e., large values of ℓ_{ec}/r , $\bar{\theta}$ is a monotonic increasing function of ϵ , so that the growth leads to an increasing detachment of the tape until it induces a complete delamination when $\bar{\theta} = \pi$. By contrast, when ℓ_{ec}/r is small, in a regime of *strong adhesion*, $\bar{\theta}$ is non-monotonic and shows a maximum value (see Figure 3). Figure 3 also shows that there is a limiting value for the excess-length ϵ below which only the adhered solution is possible. Above this threshold,

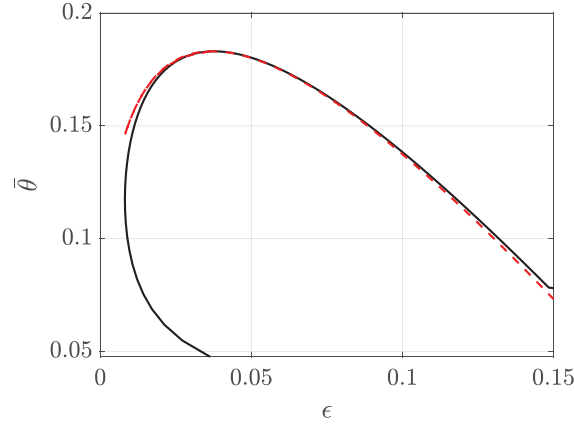


Figure 3. Detachment angle $\bar{\theta}$ versus the excess-length ϵ , with $\ell_{ec} = 0.1r$, $\ell_b = 10^{-5/2}r$. Red dashed line shows the asymptotic approximation as given in equation (59).

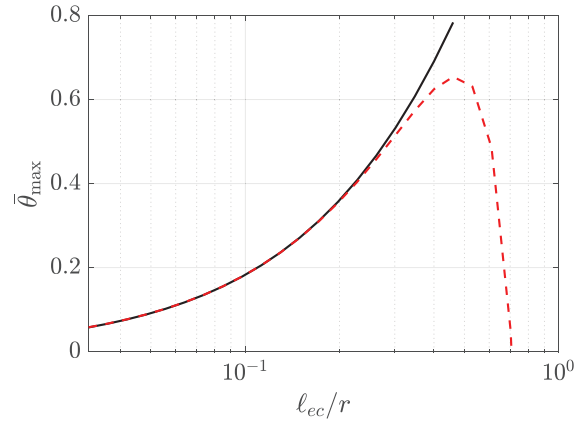


Figure 4. Maximum detachment angle as a function of ℓ_{ec} , with $\ell_b = 10^{-5/2}r$. Red dashed line shows the asymptotic approximation as given in equation (62).

the buckled solution comprises two branches (see also Figures 6 and 7) and correspondingly for one value of ϵ we can observe two buckled solutions having different sizes and different detachment angles $\bar{\theta}$. After an initial increase in delamination for small ϵ , the adhered region starts to grow again and the solution evolves from ruck to fold. Figures 4 and 5 show how the maximum detachment angle, $\bar{\theta}_{max}$, and the corresponding $\epsilon(\bar{\theta}_{max})$, depend on ℓ_{ec} .

We have explored the cases $\ell_b = 10^{-3/2}r$, and $\ell_b = 10^{-5/2}r$, that correspond to very thin films. For these values, the typical observed solutions have a delaminated part with a much longer length than ℓ_b , which implies that their compression energy is completely relaxed, i.e., $\lambda^+ \approx 1$. Hence, we can approximate the solution with that of a Euler's elastica and take advantage of its closed-form solutions and their asymptotic approximations (see Appendix 1 for details).

Figures 6 and 7 show the comparison between the energies associated with each solution branch as a function of ϵ , for $\ell_b = 10^{-3/2}r$ and two values of the elastocapillary length, namely, $\ell_{ec} = 0.1r$ and $\ell_{ec} = r$. The stored energy for the adhered configuration is easily obtained by substituting equation (29) in equation (1),

$$\frac{W_{adh}}{k/r} = -\frac{2\pi r^2}{\ell_{ec}^2} + \frac{\pi}{1+\epsilon} \left(1 + \frac{r^2 \epsilon^2}{\ell_b^2}\right), \quad (31)$$

and is shown as a red solid line. The energy associated with the partially delaminated solutions is instead calculated with a numerical simulation, drawn in blue in Figures 6 and 7. It is interesting to notice that the delaminated solution comprises two branches. The upper branch, with higher energy, corresponds to smaller rucks, whereas larger rucks correspond to the lower branch. For sufficiently small values of ϵ , only the adhered solution is found. Finally, the dashed black line in Figure 7 shows the energy of the folded solutions.

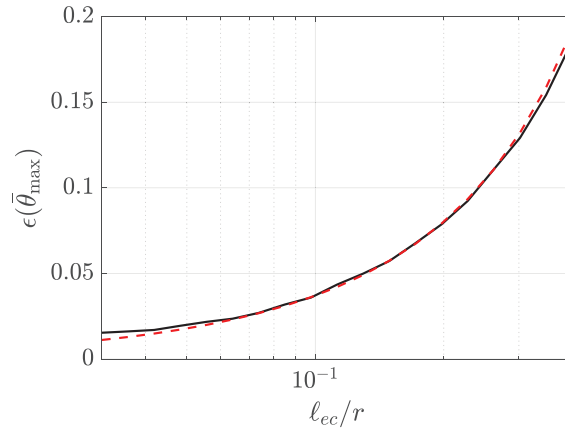


Figure 5. Maximum excess-length at detachment as a function of ℓ_{ec} , with $\ell_b = 10^{-5/2}r$. Red dashed line shows the asymptotic approximation as given in equation (61).

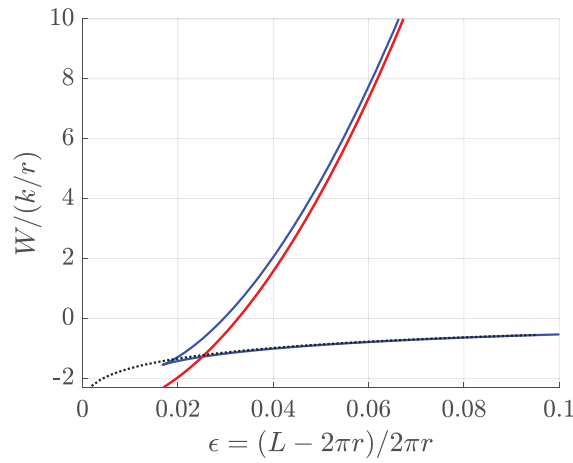


Figure 6. Energy profiles with $\ell_b = 10^{-3/2}r$, and $\ell_{ec} = r$. Black dotted line shows the energy of the inextensible case (Euler's elastica).

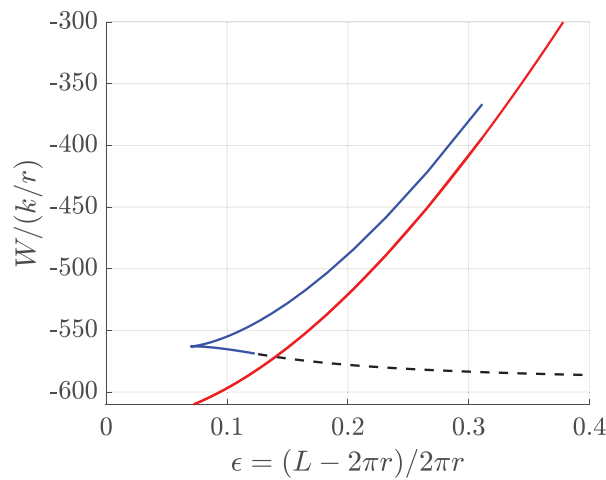


Figure 7. Energy profiles with $\ell_b = 10^{-3/2}r$, and $\ell_{ec} = 0.1r$. Black dashed line shows the energy in the folded configuration, the transition is determined by the intersection of the red line (adhered solution) with the blue/black line (corresponding respectively to the ruck/fold solutions). For this value of the parameters we observe a direct transition from the adhered solution to the fold.

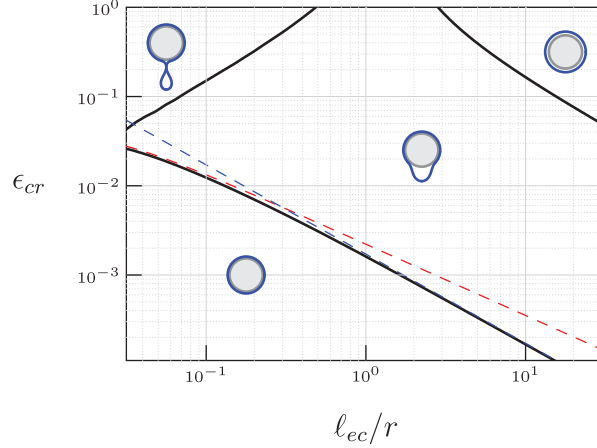


Figure 8. Phase diagram with $\ell_b = 10^{-5/2}r$. Dashed lines report the asymptotic results as given in equation (64) (dashed red line) and equation (68) (dashed blue line).

In Figure 6, we also report the energy of the delaminated solution in the inextensible case (Euler's elastica), calculated as in equation (48). As expected, when the compression reaches a critical value, the tape buckles so to relax its internal stress and compression. Thus, the buckled solution is, to a good approximation, determined by minimizing the bending energy, while the compression energy can be neglected. It is then natural to assume that the solution with $\lambda = 1$, which correctly provides the buckled shape of the beam and its energy, is also correct in the presence of a moderate adhesion potential.

From the numerical analysis with the two chosen values of ℓ_b , we identify different regions of the parameter space $(\ell_{cc}/r, \epsilon)$, shown in Figures 8 and 9, and characterized by the global minimum of the energy. The boundaries of these regions are calculated as intersections between the energy branches of the various solutions, and identify the critical values of ϵ as a function of ℓ_{cc} . For example, in Figures 6 and 7, we show the intersection between the adhered and the delaminated energy branches, corresponding to a transition from the adhered solution to a ruck (in Figure 6) or to a fold (in Figure 7). Therefore, for sufficiently small values of ℓ_{cc} , we observe that patterns of large-slope, fold-like structures may emerge directly from a uniformly compressed state, rather than grow gradually from small-slope rucks. This is in agreement with the results of Davidovitch and Démery [13], where the authors study the delamination from a flat rigid substrate under axial compression.

As can be seen from the phase diagrams in Figures 8 and 9, and from equations (64) and (68), the asymptotic approximations of ϵ_{cr} have different critical exponents in the cases of strong or weak adhesion, $\ell_{cc} \ll r$ or $\ell_{cc} \gg r$ respectively.

Furthermore, Figures 8 and 9 report also the transition lines from ruck to fold, that, for a fixed ℓ_{cc}/r , correspond to the smallest ϵ at which a self-contact of the film occurs.

Finally, the continuous line in the upper right part of the Figures 8 and 9 represents the critical threshold for the transition from buckling to complete delamination. This identifies the value of ϵ at which θ reaches π . In the inextensible case, this threshold is given in equation (42) of Napoli and Goriely [25]:

$$\epsilon_{cr}^{(\text{del})} = \frac{\sqrt{2}}{\ell_{cc}/r - \sqrt{2}}. \quad (32)$$

In the two compressible cases treated, the numerical results are not significantly different from equation (32).

5. Conclusions

We have studied the delamination induced by the growth of a compressible thin elastic sheet adhering to the outside of a cylindrical surface, due to capillary adhesion. The quasi-incompressibility assumption is consistent with very thin sheets, where ℓ_b is of the order of the sheet thickness.

We find that, due to the simultaneous presence of substrate curvature, capillary adhesion, and compressibility, the transversality condition, i.e. the additional boundary condition which serves to close the problem with unknown detachment length, is new and not obvious. This boundary condition, obtained through the classical

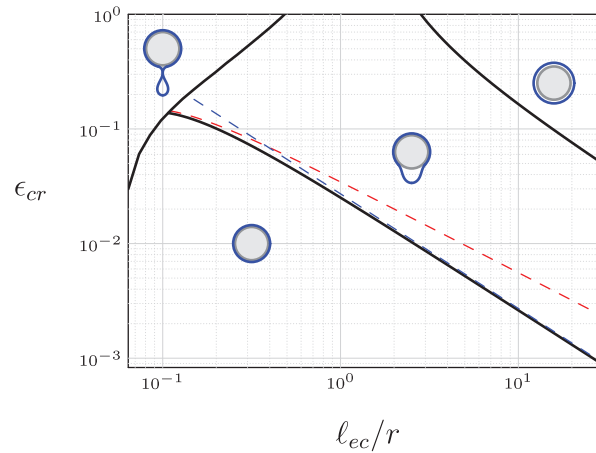


Figure 9. Phase diagram with $\ell_b = 10^{-3/2}r$. Dashed lines report the asymptotic results as given in equation (64) (dashed red line) and equation (68) (dashed blue line).

methods of calculus of variations, reduces to expressions already known in the literature in special cases. This formula can be easily generalized to the case where the film covers the interior of the cylindrical surface instead of the exterior.

Our analysis is based on the numerical resolution of a nonlinear boundary value problem. The nonlinearity of the problem results in multiple solutions whose energies are subsequently compared with each other. We assume that the branch of minimum energy is the one that is actually observed in a possible experiment.


We can summarize the results as follows. If initially the sheet length is equal to the circumference of the cylinder, the sheet adheres perfectly. During growth, there is a first stage in which the sheet, while compressing, still adheres completely to the substrate, thanks to capillary adhesion. Above a certain compression threshold, the sheet undergoes a snap-buckling, partially detaching and forming a ruck, thus releasing its compression energy. The delaminated part is effectively stretch-free. This allows us to use Euler's elastica model to approximated the solutions.

Euler's elastica offers the enormous benefit of being integrable and admitting closed-form solutions in terms of elliptic functions. Given the complexity of these functions, the obtained solutions are not immediately interpretable. However, it is possible to develop asymptotic expansions of these solutions in terms of the excess-length ϵ . In the general case, the coefficients of this asymptotic expansions are obtained from solving transcendental equations which implicitly involve the characteristic lengths ℓ_b , ℓ_{cc} , and r . However, in both the strong adhesion limit $\ell_{cc} \ll r$ and the weak adhesion limit $\ell_{cc} \gg r$, it is possible to explicitly find these coefficients. This allows us to find useful asymptotic laws that relates the geometrical and material features of the problem. The success of these asymptotic results could be very useful in interpreting experimental results or in helping to design targeted experiments. For example, we are able to capture the critical thresholds for the onset of ruck solutions (see equations (64) and (68)), in perfect agreement with numerical simulations.

Funding

The author(s) disclosed receipt of the following financial support for the research, authorship, and/or publication of this article: This work was supported by the by the MIUR Project PRIN 2020, "Mathematics for Industry 4.0", Project No. 2020F3NCPX, and also conducted under the auspices of the GNFM-INdAM.

ORCID iD

Gaetano Napoli  <https://orcid.org/0000-0002-0539-2686>

References

- [1] Sun, Y, Choi, WM, Jiang, H, et al. Controlled buckling of semiconductor nanoribbons for stretchable electronics. *Nature Nanotech* 2006; 1(3): 201–207.

- [2] Vella, D, Bico, J, Boudaoud, A, et al. The macroscopic delamination of thin films from elastic substrates. *Proc Natl Acad Sci USA* 2009; 106(27): 10901–10906.
- [3] Lu, N, and Kim, DH. Flexible and stretchable electronics paving the way for soft robotics. *Soft Rob* 2013; 1(1): 53–62.
- [4] Box, F, Domino, L, Corvo, TO, et al. Delamination from an adhesive sphere: curvature-induced dewetting versus buckling. *Proc Natl Acad Sci* 2023; 120(12): e2212290120, <https://www.pnas.org/doi/abs/10.1073/pnas.2212290120>
- [5] Gioia, G, and Ortiz, M. Random blisters on stickers: metrology through defects. *Adv Appl Mech* 1997; 33: 19–192.
- [6] Aoyanagi, Y, Hure, J, Bico, J, et al. Random blisters on stickers: metrology through defects. *Soft Matter* 2010; 6: 5720–5728.
- [7] Cohen, AE, and Mahadevan, L. Kinks, rings, and rackets in filamentous structures. *Proc Natl Acad Sci U S A* 2003; 100(21): 12141.
- [8] Glassmaker, NJ, and Hui, CY. Elastica solution for a nanotube formed by self-adhesion of a folded thin film. *J Appl Phys* 2004; 96(6): 3429–3434.
- [9] Chen, JS, and Li, CW. Planar elastica inside a curved tube with clearance. *Int J Solids Struct* 2007; 44(18): 6173–6186, <https://www.sciencedirect.com/science/article/pii/S0020768307000893>
- [10] Cerda, E, and Mahadevan, L. Confined developable elastic surfaces: cylinders, cones and the elastica. *Proc R Soc A* 2005; 461(2055): 671–700.
- [11] Wagner, TJW, and Vella, D. The ‘sticky elastica’: delamination blisters beyond small deformations. *Soft Matter* 2013; 9(4): 1025–1030.
- [12] Napoli, G, and Turzi, S. The delamination of a growing elastic sheet with adhesion. *Meccanica* 2017; 52(14): 3481–3487.
- [13] Davidovitch, B, and Démery, V. Rucks and folds: delamination from a flat rigid substrate under uniaxial compression. *Eur Phys J E* 2021; 44(2): 11.
- [14] Oshri, O, Liu, Y, Aizenberg, J, et al. Delamination of a thin sheet from a soft adhesive winkler substrate. *Phys Rev E* 2018; 97: 062803.
- [15] Yuan, X, Zhu, B, and Wang, Y. Post-buckling evolution of compressed thin films adhered to rigid substrates. *Int J Mech Sci* 2022; 232: 107616, <https://www.sciencedirect.com/science/article/pii/S0020740322005033>
- [16] Rim, JE, Purohit, PK, and Klug, WS. Mechanical collapse of confined fluid membrane vesicles. *Biomech Model Mechan* 2014; 13(6): 1277–1288.
- [17] Napoli, G, and Turzi, S. Snap buckling of a confined thin elastic sheet. *Proc R Soc A* 2015; 471(2183): 20150444.
- [18] Napoli, G, and Goriely, A. A tale of two nested elastic rings. *Proc Math Phys Eng Sci* 2017; 473(2204): 20170340.
- [19] De Tommasi, D, Devillanova, G, Maddalena, F, et al. Elastic multi-blisters induced by geometric constraints. *Proc Math Phys Eng Sci* 2021; 477(2245): 20200562, <https://royalsocietypublishing.org/doi/abs/10.1098/rspa.2020.0562>
- [20] Boué, L, Adda-Bedia, M, Boudaoud, A, et al. Spiral patterns in the packing of flexible structures. *Phys Rev Lett* 2006; 97(16): 166104.
- [21] Goriely, A. *The mathematics and mechanics of biological growth*. New York: Springer, 2017.
- [22] O’Reilly, OM. A material momentum balance law for rods. *J Elast* 2007; 86: 155–172.
- [23] O’Reilly, OM. *Modeling nonlinear problems in the mechanics of strings and rods*. Berlin: Springer, 2017.
- [24] De Pascalis, R, Napoli, G, and Turzi, SS. Growth-induced blisters in a circular tube. *Phys D* 2014; 283: 1–9.
- [25] Napoli, G, and Goriely, A. Elastocytosis. *J Mech Phys Solids* 2020; 145: 104133, <https://www.sciencedirect.com/science/article/pii/S0022509620303677>
- [26] Abramowitz, M, and Stegun, IA. *Handbook of mathematical function with formulas, graphs, and mathematical tables*. New York: Dover, 1964.

Appendix I

The inextensible case

When inextensibility of the tape is assumed, i.e., $\lambda \equiv 1$ everywhere, the equations to solve reduce to

$$\frac{k}{\bar{S}^2} \theta_{\sigma\sigma} - n_x \sin \theta = 0, \quad (33a)$$

$$x_\sigma = \bar{S} \cos \theta, \quad (33b)$$

where the subscript σ indicates differentiation with respect to the rescaled variable $\sigma := S/\bar{S} \in [0, 1]$.

The boundary conditions can be written as

$$\theta(0) = 0, \quad \theta(1) = \bar{\theta}, \quad (34a)$$

$$x(0) = 0, \quad x(1) = \bar{S} \sin \bar{\theta}, \quad (34b)$$

while the transversality condition reduces to

$$\theta_\sigma(1) = \bar{S} \left(\frac{1}{r} - \frac{\sqrt{2}}{\ell_{ec}} \right). \quad (35)$$

Note that equation (33a) looks like nonlinear pendulum equation and, hence, its solution can be given in closed form in terms of integrals and elliptic functions. We refer the reader to the book [26] for notation.

Equation (33a) admits the first integral

$$\frac{1}{2} \frac{k}{\bar{S}^2} \theta_\sigma^2 + n_x \cos \theta = C := \frac{1}{2} \frac{k}{\bar{S}^2} \kappa_0^2 + n_x,$$

where $\kappa_0 := \dot{\theta}(0)$, whence

$$\theta_\sigma^2 = \kappa_0^2 \left[1 - \frac{4\bar{S}^2 |n_x|}{k\kappa_0^2} \sin^2 \frac{\theta}{2} \right]. \quad (36)$$

We define

$$m := \frac{4\bar{S}^2 |n_x|}{k\kappa_0^2}, \quad (37)$$

and look for solution where $\kappa_0 > 0$, so that from equation (36) we get

$$\theta_\sigma = \kappa_0 \sqrt{1 - m \sin^2 \frac{\theta}{2}}.$$

Thus, we can separate the variables and then integrate, obtaining

$$F\left(\frac{\theta}{2}; m\right) = \frac{\kappa_0}{2} \sigma,$$

with $F(\cdot)$ denoting the elliptic integral of first kind, whence

$$\theta(\sigma) = 2 \operatorname{am}\left(\frac{\kappa_0}{2} \sigma, m\right), \quad (38)$$

where $\operatorname{am}(\cdot)$ denotes the Jacobi amplitude. Consequently, the boundary condition (34a)₂ yields

$$\bar{\theta} = 2 \operatorname{am}\left(\frac{\kappa_0}{2}, m\right), \quad (39)$$

whereas the transversality condition (35) reduces to

$$\frac{\bar{S}}{r} \left(1 - \frac{\sqrt{2}r}{\ell_{ec}} \right) = \kappa_0 \operatorname{dn}\left(\frac{\kappa_0}{2}, m\right). \quad (40)$$

Using equation (38), (33b) reduces to

$$x_\sigma = \bar{S} \left[1 - 2 \operatorname{sn}^2\left(\frac{\kappa_0}{2} \sigma, m\right) \right], \quad (41)$$

that can be integrated yielding

$$x(\sigma) = \bar{S} \left[\left(1 - \frac{2}{m} \right) \sigma + \frac{4}{m\kappa_0} E\left(\frac{\kappa_0}{2} \sigma, m\right) \right], \quad (42)$$

where

$$E(u, m) := \int_0^u \operatorname{dn}^2(t, m) dt \quad (43)$$

is the incomplete elliptic integral of second kind. Consequently, the boundary condition (34b)₂ becomes

$$\sin \bar{\theta} = \frac{\bar{S}}{r} \left[\left(1 - \frac{2}{m} \right) + \frac{4}{m\kappa_0} E \left(\frac{\kappa_0}{2}, m \right) \right]. \quad (44)$$

Notice that the inextensibility condition provides the relationship between \bar{S} and $\bar{\theta}$:

$$\frac{\bar{S}}{r} = \pi \left(\frac{L}{2\pi r} - 1 \right) + \bar{\theta}. \quad (45)$$

Equations (39), (40), (44), and (45), provide a system of four transcendental algebraic equation for the four dimensionless unknowns $\bar{\theta}$, \bar{S}/r , κ_0 , and m .

Finally, the total free energy is (see equation (1))

$$\begin{aligned} \frac{W}{k/r} &= \frac{r}{k} \left[k \int_0^{\bar{S}} \theta'^2 ds + \int_{\bar{S}}^{L/2} \left(\frac{k}{r^2} - 2 \frac{k}{\ell_{ec}^2} \right) ds \right] \\ &= \frac{2\kappa_0 r}{\bar{S}} E \left(\frac{\kappa_0}{2}, m \right) + \left(1 - 2 \frac{r^2}{\ell_{ec}^2} \right) (\pi - \bar{\theta}). \end{aligned} \quad (46)$$

It should be noted that the solutions presented so far apply when $0 \leq m \leq 1$. Conversely, when $m > 1$ the solutions still apply provided the following substitutions are made (see Abramowitz and Stegun [26]):

$$\operatorname{sn}(u, m) = \frac{1}{\sqrt{m}} \operatorname{sn} \left(\sqrt{m} u, \frac{1}{m} \right), \quad (47a)$$

$$\operatorname{cn}(u, m) = \operatorname{dn} \left(\sqrt{m} u, \frac{1}{m} \right), \quad (47b)$$

$$\operatorname{dn}(u, m) = \operatorname{cn} \left(\sqrt{m} u, \frac{1}{m} \right), \quad (47c)$$

$$E(u, m) = \sqrt{m} E \left(\sqrt{m} u, \frac{1}{m} \right) - (m - 1)u \quad (47d)$$

and the energy expression becomes

$$\frac{W}{k/r} = \frac{2\kappa_0 r}{\bar{S}} \left[\sqrt{m} E \left(\frac{1}{2} \sqrt{m} \kappa_0, \frac{1}{m} \right) - (m - 1) \frac{\kappa_0}{2} \right] + \left(1 - 2 \frac{r^2}{\ell_{ec}^2} \right) (\pi - \bar{\theta}). \quad (48)$$

Asymptotic results. Geometrically, we expect the quantities $\bar{\theta}$, κ_0 and \bar{S}/r to be infinitesimal when ϵ , defined in equation (30), approaches zero. Furthermore, $\bar{\theta}$ and \bar{S}/r have the same asymptotic behavior, as can be seen from equation (45). Finally, from the analysis of equation (40) (or its correspondent using equation (47)), it can be seen that κ_0 has the same asymptotic behavior as \bar{S}/r . This, in turn, implies that m has the same asymptotic of n_x (see equation (37)) which, on physical ground, one expects to be unbounded when $\epsilon \rightarrow 0$.

In summary, whenever $m > 1$, we have to use the correspondence (47) to rewrite the boundary conditions (39), (40), (44), and (45), respectively, as

$$\sin(\bar{\theta}/2) = \frac{1}{\sqrt{m}} \operatorname{sn} \left(\sqrt{m} \frac{\kappa_0}{2}, \frac{1}{m} \right), \quad (49a)$$

$$\frac{\bar{S}}{r} \rho = \kappa_0 \operatorname{cn} \left(\sqrt{m} \frac{\kappa_0}{2}, \frac{1}{m} \right), \quad (49b)$$

$$\sin \bar{\theta} = \frac{\bar{S}}{r} \left[\frac{4}{\sqrt{m}\kappa_0} E \left(\sqrt{m} \frac{\kappa_0}{2}, \frac{1}{m} \right) - 1 \right], \quad (49c)$$

$$\frac{\bar{S}}{r} = \bar{\theta} + \pi \epsilon. \quad (49d)$$

where we introduced the abbreviation $\rho := 1 - \sqrt{2}r/\ell_{ec}$.

Equation (49a) suggests that $\bar{\theta} \sim \epsilon^q$ and $m \sim \epsilon^{-2q}$ for some $q > 0$. Using the small modulus expansion of the elliptic integral

$$E(u, \lambda) = u + \frac{\lambda}{2}(\cos(u) \sin(u) - u) + O(\lambda^2), \quad (50)$$

and comparing $\sin \bar{\theta}/(\bar{S}/r)$ with the term in the square parenthesis in equation (49c), we find that $q = 1/3$.

The analysis can be made more precise assuming

$$m = \sum_{j \geq -2} \mu_j \epsilon^{j/3}, \quad \kappa_0 = \sum_{j \geq 1} \tau_j \epsilon^{j/3}, \quad \bar{\theta} = \sum_{j \geq 1} \alpha_j \epsilon^{j/3}, \quad (51)$$

and using equation (49d) for \bar{S}/r .

Substituting these expansions into equation (49), with the help of small-modulus expansion of the elliptic functions (see 16.23 of Abramowitz and Stegun [26]) we obtain, for each power $\epsilon^{j/3}$, a system of transcendental equations for the related coefficients μ_j , τ_j , and α_j .

The first non-zero conditions are obtained for $j = 1$ and read

$$\alpha_1 \rho = \tau_1 \cos\left(\frac{1}{2}\sqrt{\mu_{-2}} \tau_1\right), \quad \alpha_1 = 2 \frac{1}{\sqrt{\mu_{-2}}} \sin\left(\frac{1}{2}\sqrt{\mu_{-2}} \tau_1\right). \quad (52)$$

By introducing $\xi := \sqrt{\mu_{-2}} \tau_1/2$, these relations reduce to

$$\tan \xi = \frac{\xi}{\rho}, \quad (53)$$

which, for a given ρ , has infinitely many solutions.

Let us denote the chosen solution by ξ_* , we can write

$$\alpha_1 = \frac{2}{\sqrt{\mu_{-2}}} \sin \xi_*, \quad \tau_1 = \frac{2}{\sqrt{\mu_{-2}}} \xi_*. \quad (54)$$

The procedure is conceptually simple, but the algebra needed for $j \geq 2$ becomes soon so much cumbersome and involved that we prefer to report only the results. For $j = 2$ for example we obtain that

$$\alpha_2 = -\frac{\mu_{-1}}{(\mu_{-2})^{3/2}} \sin \xi_*, \quad \tau_2 = -\frac{\mu_{-1}}{(\mu_{-2})^{3/2}} \xi_*. \quad (55)$$

For $j = 3$ we found that

$$\mu_{-2} = \left[\frac{2 \sin \xi_*}{\pi} \left(1 - \frac{2\xi_*^2 + 3\rho}{3\xi_*^2} \sin^2 \xi_* \right) \right]^{2/3}, \quad (56)$$

which also allows us to obtain a closed expression for α_1 and τ_1 . Furthermore, we found that α_3 and τ_3 are linear functions of μ_0 .

Finally, for $j = 4$, we found that $\mu_{-1} = 0$ and therefore also $\alpha_2 = \tau_2 = 0$, while α_4 and τ_4 are proportional to μ_1 .

Strong adhesion regime.

When the adhesion energy is dominant, we $\ell_{ec} \ll r$, so that $\rho \rightarrow -\infty$. As a solution to the equation (53) we get, up to $O(\rho^{-2})$,

$$\xi_*^{(\infty)} = \pi(1 + \rho^{-1} + \rho^{-2}), \quad (57)$$

where the superscript (∞) stands for strong adhesion regime. Consequently, we get

$$\mu_{-2}^{(\infty)} = \left(\frac{2}{\rho}\right)^{2/3} \left(1 - \frac{7\pi^2}{9}\rho^{-2} + O(\rho^{-3})\right). \quad (58)$$

We obtain the following asymptotic expression for $\bar{\theta}$:

$$\bar{\theta}^{(\infty)} \approx \alpha_1^{(\infty)} \epsilon^{\frac{1}{3}} + \alpha_3^{(\infty)} \epsilon + \alpha_5^{(\infty)} \epsilon^{\frac{5}{3}} \quad (59)$$

with

$$\alpha_1^{(\infty)} := 2^{\frac{2}{3}} \pi (\rho^{-\frac{2}{3}} + \rho^{-\frac{5}{3}}), \quad \alpha_3^{(\infty)} := -\frac{7}{8} \pi (1 + \rho^{-1}), \quad \alpha_5^{(\infty)} := \frac{2^{\frac{1}{3}}}{64} \pi \rho^{\frac{2}{3}}. \quad (60)$$

The function $\bar{\theta}^{(\infty)}$ reaches its maximum at

$$\epsilon_{\max}^{(\infty)} \approx -0.4871 \rho^{-1} + 0.0178 \rho^{-2}, \quad (61)$$

at which

$$\bar{\theta}_{\max}^{(\infty)} \approx -2.6035 \rho^{-1} - 2.5848 \rho^{-2}. \quad (62)$$

Similarly, we obtain the expansion of the total energy

$$\frac{W}{k/r} \approx -\frac{\pi}{\rho^2} (1 - 2\rho^{-1}) + 3 \cdot 2^{-\frac{1}{3}} \pi \epsilon^{1/3} - \frac{5\pi}{8} \rho^2 \epsilon. \quad (63)$$

When the energy of the fully adhered solution exceeds the energy of the partially delaminated branch, delamination occurs. Thus, the intersection between the energies (63) and (31) provides an estimate of the critical threshold at which this transition occurs, within the strong adhesion regime. We thus obtain the asymptotic threshold:

$$\epsilon_{\text{cr}}^{(\infty)} \approx \left(\frac{54 \ell_b^6}{\ell_{\text{ec}}^4 r^2} \right)^{\frac{1}{3}} - \frac{3}{4} \left(\frac{\ell_b^6}{\ell_{\text{ec}}^4 r^2} \right)^{\frac{1}{3}}. \quad (64)$$

Weak adhesion regime.

Let consider the interesting limit of weak adhesion, that is, $\ell_{\text{ec}} \ll r$ meaning that one can write $\rho = 1 - \eta$, with

$$\eta := \frac{\sqrt{2}r}{\ell_{\text{ec}}} \rightarrow 0. \quad (65)$$

Within this regime of parameters, the appropriate solutions are those with $m < 1$. A simple analysis of equation (53) shows that the first positive solution can be written as

$$\xi_* = \sqrt{3\eta} \left(1 - \frac{\eta}{10} + \frac{9\eta^2}{1400} + O(\eta^3) \right). \quad (66)$$

For this case, we only report the asymptotic expression of the energy

$$\frac{W}{k/r} \approx \pi (1 - \eta^2) + \frac{3}{5} (15\pi)^{\frac{1}{3}} \eta^{\frac{5}{3}} - \pi \epsilon. \quad (67)$$

By comparison between equations (67) and (31), we obtain the asymptotic expression of the threshold, in the weak adhesion limit, at which the ruck arises:

$$\epsilon_{\text{cr}}^{(0)} \approx 1.7154 \left(\frac{\ell_b}{r} \right)^{\frac{6}{5}} \frac{r}{\ell_{\text{ec}}}. \quad (68)$$